Lasers in Manufacturing Conference 2021

Influence of multi-pass laser hardening on residual stress and distortion

Yang Lu[a,*], Heiner Meyer[b], Tim Radel[a]

[a]*BIAS - Bremer Institut für angewandte Strahltechnik GmbH, Klagenfurter Str. 5, 28359 Bremen, Germany*
[b]*Leibniz-Institut für Werkstofforientierte Technologien, Badgasteiner Str. 3, 28359 Bremen, Germany*

Abstract

Laser hardening is used to harden the surface layer with minimal distortion and to induce residual compressive stresses. Within the literature, the approach of increasing the hardness and hardening depth by multi-pass laser hardening based on accumulation effects is shown. In this study, the effect of this approach is investigated on the residual stresses and distortion of normalized AISI 4140. The multi-pass laser hardening is carried out using a continuous wave laser with a rectangular beam shape using different process velocities and number of passes without heat accumulation between each pass. The results show that the compressive residual stresses at the surface slightly decrease with number of passes. Meanwhile the compressive residual stresses in the depth of the hardened zone increase with number of passes, along with an increase of the width (FWHM) of the diffraction peak in XRD spectrum. Nevertheless, for a comparable hardening depth, there is less distortion at one-cycle phase transformation with low scanning speed compared to the multi-cycle phase transformation with higher scanning speed. These findings indicate that multi-pass laser hardening could be beneficial for industrial application due to a larger phase-transformed zone with higher compressive residual stresses in depth and larger hardening depth, if the increased distortion is acceptable.

Keywords: Laser hardening; Multi-pass hardening, Phase transformation, Residual stress, Distortion

1. Introduction

Laser hardening is a process to increase hardness and introduce compressive residual stresses of the hardenable steel, which further improves the lifetimes of the engineering components. The increase of the hardness is due to the generation of martensite and the compressive residual stresses is mainly due to the

* Corresponding author. Tel.: +49-421-218-58046; fax: +49-421-218-58063 .
E-mail address: lu@bias.de .

resultant volume expansion of martensite, and the mechanisms are intensively studied numerically and experimentally in the past decades [Nat18].

In terms of residual stresses, they can be divided into macroscopic (polycrystal), microscopic (within grains) and submicroscopic stresses based on the scope of the action, and the first and second kind can be measured non-destructively by X-ray diffraction (XRD) [Epp16]. An ideal and perfect single crystal lattice is represented as a narrow, symmetrical and delta-function like peak in an XRD spectrum [Ung04]. However, due to different sources of strain, such as dislocations, microstresses and internal stresses, the XRD pattern differ from the ideal one due to different peak aberrations, consisting of peak shift, peak broadening, peak asymmetries and peak shape [Ung04]. Here peak shift and peak broadening share several sources of strain, for example stacking faults, grain boundaries and chemical heterogeneities, while the peak shift is additionally related to the different type of internal macrostresses (compressive or tensile) [Epp16], and the peak broadening is elsewise attributed to the dislocations, microstresses, crystallite smallness and stress gradient [Ung04].

In the single-pass laser hardening, residual stresses generation is mainly attributed to the rapid thermal heating and constrained cooling due to the clamping specimen, and the magnitude of these stresses depends on the type of processing, temperature gradient and phase-change kinetics [Bab19]. Therefore, whether thermal strains or phase transformation strains are dominant, their relationship determines the resulting stresses. The residual stress profile along depth consists of the compressive residual stresses in the hardened zone and compensating tensile stress in the base material underneath [Bab19]. The compressive stress is mainly due to the volumetric dilatation induced by austenite-martensite transformation, while the tensile stress is due to compensation of the layer stress to a macroscopic zero stress state aside from distortion. In the hardened zone, the generation of martensite was found to have a greater influence than the thermal strain [Bab19]. Recently an in-situ synchrotron XRD analysis of laser hardening separated thermal and elastic strains and identified the effects of phase transformation, quenching and mechanical constraint from cold base material underneath the laser hardened zone [Kos17]. Based on this, it is revealed that the compressive residual stresses developed due to the local compressive elasto-plastic deformations and local specific transformation strains, while the tensile stresses outside the hardened zone is originated from the superposition of quenching effects, local elasto-plastic deformation and the phase transformation effect [Kos17].

Furthermore, laser hardening with multi-cycle phase transformation were investigated to enhance the conventional limitation of single pass laser hardening such as limited soaking time and thickness of the hardened layer [Nat18]. Besides the enhanced hardened zone and hardness, a decrease of surface compressive residual stress in multi-pass laser hardening of quenched and tempered (QT) AISI 4140 was observed in several studies. For example, a simultaneous grain coarsening in the near surface was observed in [Mio05] and an extension of compressive residual stress zone along depth was observed in [Kos11]. Furthermore, besides the QT steel, the residual stress decrease at the surface was also observed for the soft annealed and normalized one [Lu20]. The evolution of residual stress distribution was assumed to be the result of the superposition of phase transformation, quenching effects and local residual stresses from previous pass [Kos11].

Besides the residual stress, plastic deformation or distortion is the result of sliding dislocation within a crystal structure [Kuh89]. In the macroscopic level, the involved plastic deformation is because thermal stress is larger than the yield stress of the material. In terms of laser hardening, the distortion of workpiece should depend on surface stability, laser processing parameters and residual stress distribution in the surface layer, and the distortion is comparatively small [Nat18]. However, only laser hardened gears with low quality can be used directly without postprocessing of grinding, which implies the distortion of laser hardened steel for high accuracy class cannot be neglected [Zha03].

Based on the state of the research, multi-pass laser hardening has been investigated regarding the hardness, which show potential for the industrial applications as the hardening depth increases. However, it is not clear how this process using continuous wave laser influences the residual stresses in depth and the distortion, which is aimed to be investigated in this paper.

2. Methods

2.1. Laser hardening

Multi-pass laser hardening of normalized AISI 4140 with repetition of 1, 2, 4, 8 and 16 passes was conducted by using a continuous wave disc laser (TruDisk 12002, Trumpf GmbH) at the scanning speed of 5 mm/s, 10 mm/s and 20 mm/s. The laser power was set in each pass, so that all the specimens have been irradiated with a maximum surface temperature of 1400 °C in each pass, which was measured by a two-color pyrometer (IGAR 12-LO MB 22, LumaSense Technologies GmbH). The other laser parameters are listed in Fig. 1. During the process, heat accumulation effect was avoided by fixing the workpiece between water-cooled copper clamps. Moreover, the following heating cycles were initiated after the workpiece temperature was cooled down to the room temperature. The process surface was protected by argon shielding gas.

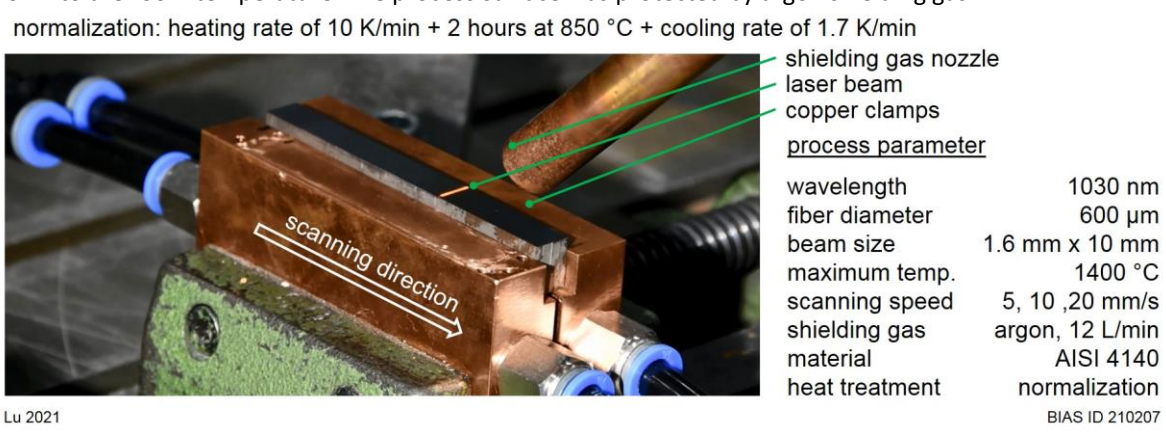

Fig. 1. Multi-pass laser hardening using rectangular beam shape

2.2. Characterization

For the distortion investigation, a three-dimensional (3-D) measurement system (CRYSTA-APEX C, Mitutoyo GmbH) was applied to obtain profiles of the laser treated surface before and after laser hardening. This was realized by recording the coordinates of several parallel lines on the surface, with the orientation parallel to the laser scanning direction. Afterwards the exported data from the correlated controlling software (MCOSMOS, Mitutoyo GmbH) were postprocessed by Matlab (R2018a, Matlab) to calculate the distortion. The bending of the cuboid sample is represented by a peak-valley value of laser treated surface, which scheme is shown in Fig. 2.

Residual stress state on the surface and in depth was measured using an X-ray diffractometer (XRD) with a θ-2θ type Goniometer Seifert MZ IV and chromium radiation. Measurements were performed in two orthogonal directions (0°) in feed direction and (90°) perpendicular to feed direction. The $\sin^2\psi$-method [Epp16] and X-ray elastic constants E = 220000 MPa and ν = 0.28 [Noy87] were used to determine the

stress under assumption of normal stress σzz = 0. The α{211}-crystallographic planes were analyzed and additionally the Full width at half-maximum (FWHM) of the diffraction peak was given. Main measurement parameters are given in Table 1. Depth measurements were performed after stepwise surface removal using electropolishing between every measurement with an electrolyte of phosphoric and nitric acid.

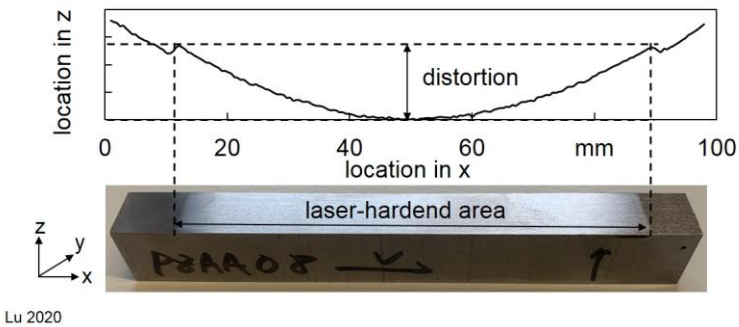

process parameter

wavelength	1030 nm
beam size	1.6 mm (1/e) x 10 mm
surface max. temp.	1400 °C
shielding gas	argon, 12 L/min
material	AISI 4140, normalized
geometry	100 x 10 x 13 mm³

profile measurement

machine	CRYSTA-APEX C

BIAS ID 201048

Fig. 2. Exemplary scheme for characterizing the distortion of the laser treated surface

Table 1. Measurement parameters for XRD

Line Detector	Primary Beam	Lattice plane	Tube voltage/ current	2θ angles	Step ψ angles
Photron-X Miostar	Ø 2 mm	α{211}	33 kV/40 mA	147°-163°	0.1° from -45° to +45°

To observe the metallographic microstructure, the longitudinal section was polished and etched by Nital for a few seconds. After the preparation of optical micrographs, Vickers hardness test (Emco-Test) was carried out with an applied load of 2 N in the framework of ISO 6507-1 for three times. In this study laser-affected zone is defined and divided into hardened zone (HZ) and transition zone (TZ) in sequence along the depth direction, followed by the unaffected base material (BM) [Bab19]. The hardening depth is determined as the distance from the surface at which the hardness values first reach the hardness of the base material.

3. Results

3.1. Hardness and microstructure

Fig. 3 presents the depth profile of hardness and the microstructure of the hardened zone (HZ), transition zone (TZ) and base material (BM) based on different number of passes and scanning speed in multi-pass laser hardening. For the effect of number of passes, the hardness in the hardening zone after the first treatment does not reach the maximum compared to 16 passes. At 16 passes, the hardness in the hardened zone reaches the maximum value. Additionally, there is an increase of hardening depth and increased phase transformed zone. Compared to the single pass, finer microstructure near the bottom is identified and the boundary between the transition zone and base material is more differentiated. In addition, needle-like martensite microstructure is only easily visible near the surface after cyclic phase transformation. Based on the experiment design, the maximum surface temperature for all the scanning speeds is controlled around 1400 °C. Nevertheless, all of specimens have increased hardness and hardening depth at 16-pass hardening.

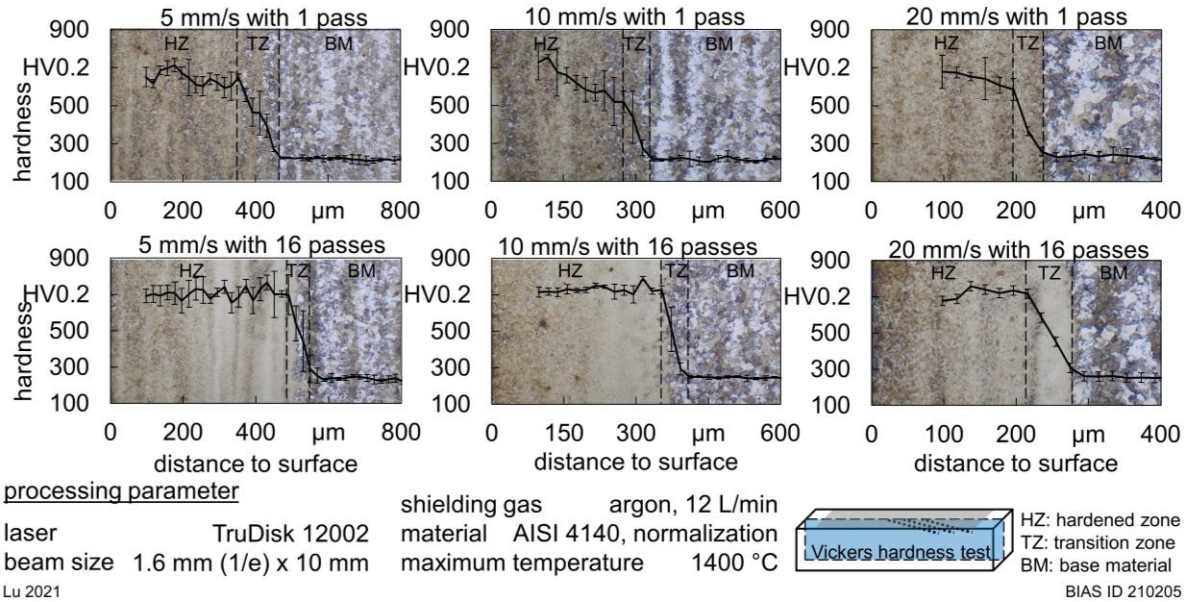

Fig. 3. Depth profile of hardness and microstructure after single and multi-pass laser hardening of normalized AISI 4140

3.2. Residual stress

In Fig. 4 the results of XRD analysis are presented and shows the surface residual stresses and FWHM of the peak in the XRD spectrum along feed direction (0°) and orthogonal direction (90°) as input state and at 1, 2, 4, 8 and 16 passes of laser hardening. The ground surface before and after laser hardening shows compressive residual stresses condition in both directions. The maximum surface residual stresses for both directions are observed after the first irradiation. During the following repetitions, the surface residual stresses show a decreasing tendency with each pass. For the FWHM of the diffraction peak, the value at the first pass increases significantly. Although the value fluctuates in the following treatment, at 16 passes it shows a decreasing trend, and there is negligible difference in both measured directions for all the scanning speeds.

Compared to the surface modification, the depth profile of residual stresses and FWHM of the diffraction peak for scanning speed of 10 mm/s and 20 mm/s are presented in 0° (Fig. 5) and 90° (Fig. 6), and the corresponding results for both measuring directions are quite similar. By comparing with the hardness profile in Fig. 3, at the first pass there are as expected compressive residual stresses in the hardened zone, followed by a transfer of stress from the compressive to the tensile underneath. In the base material there are tensile residual stresses. In the multi-pass laser hardening, different from the results in Fig. 4, the compressive residual stresses and FWHM of diffraction peak in the depth between 100 µm and 300 µm increase with number of passes. It is worth noting that, at the 16 cycles of phase transformation compared to the single pass, the increased region with compressive residual stress is much larger for the scanning speed of 20 mm/s compared to 10 mm/s.

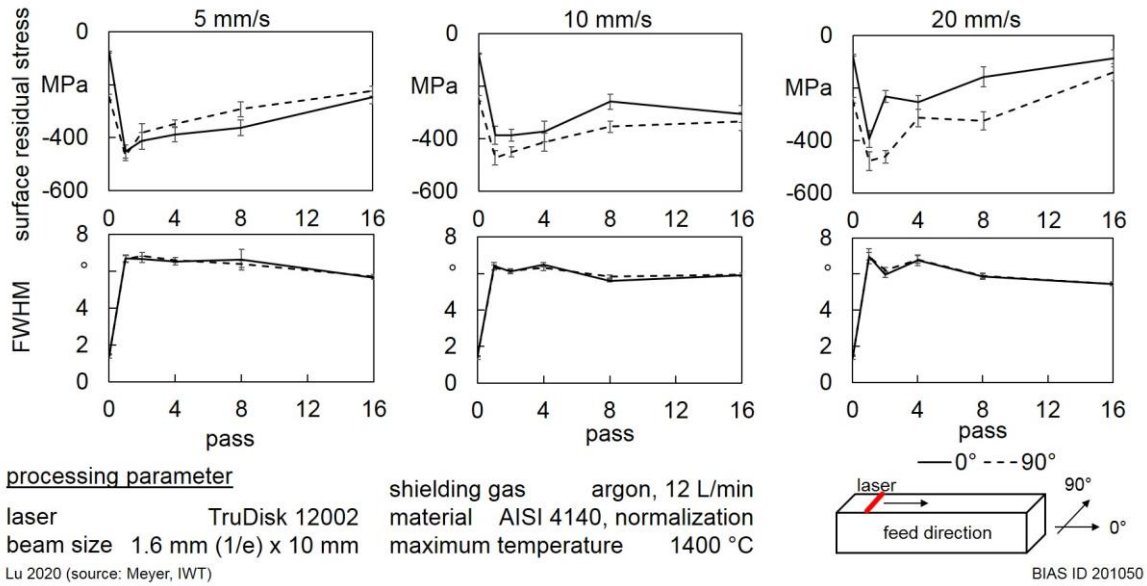

Fig. 4. Residual stress and FWHM of diffraction peak in the XRD spectrum after single and multi-pass laser hardening of normalized AISI 4140

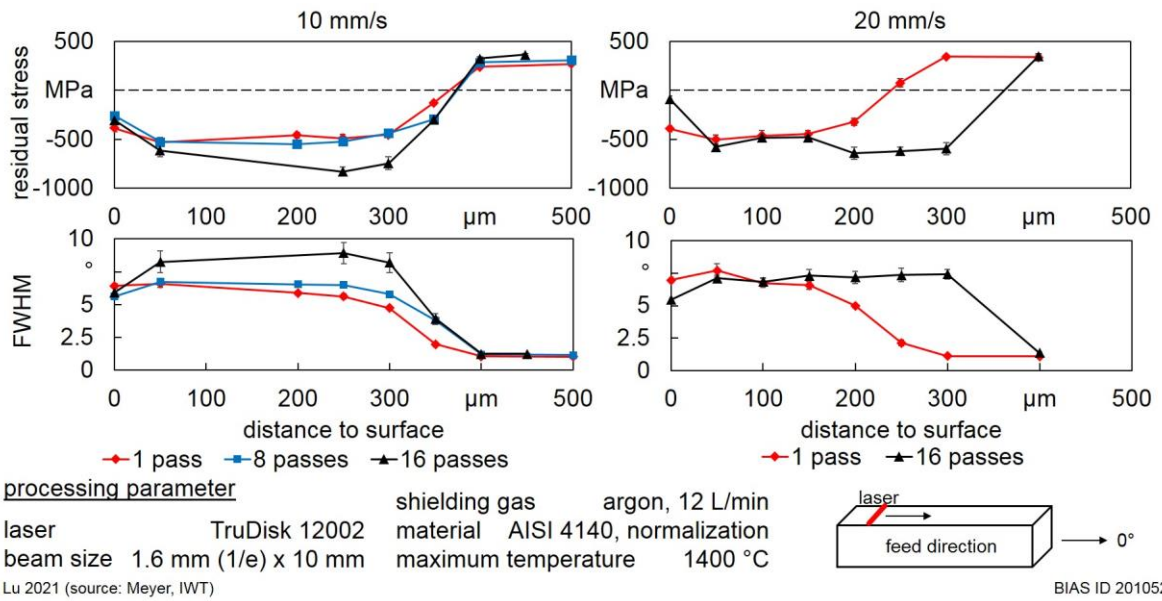

Fig. 5. Depth profile of residual stress and FWHM of diffraction peak after single and multi-pass laser hardening of normalized AISI 4140, with XRD measurement in 0°

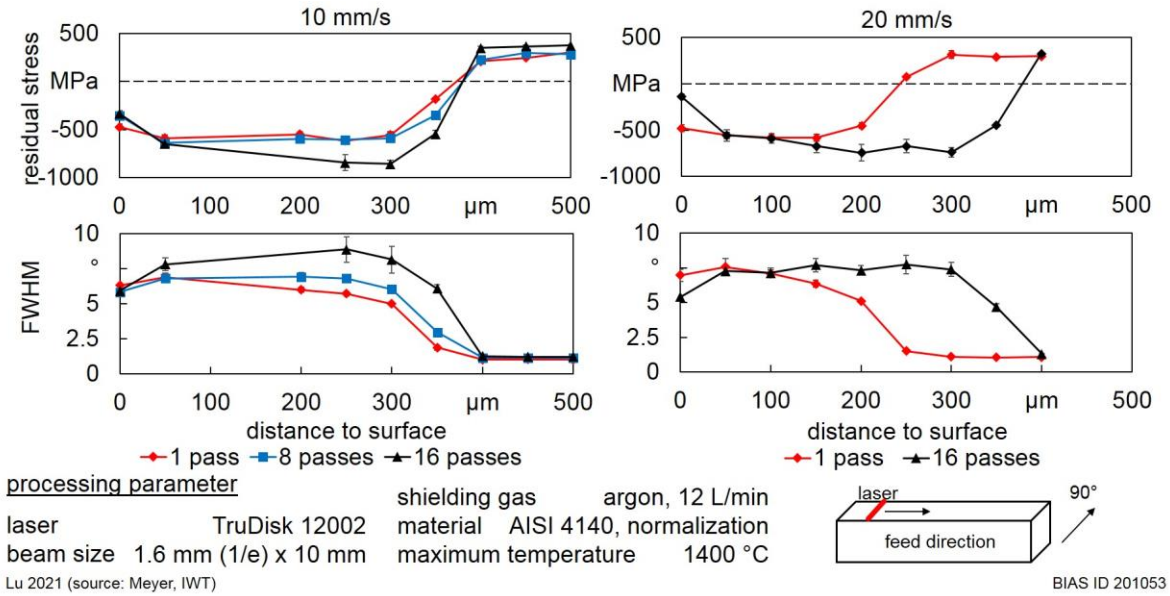

Fig. 6. Depth profile of residual stress and FWHM of diffraction peak after single and multi-pass laser hardening of normalized AISI 4140, with XRD measurement in 90°

3.3. Distortion

Based on the hardness measurement for different parameter and number of passes, two groups of parameter combination (scanning speed with number of passes) with comparable hardening depth (the first group: 5 mm/s with 1 pass and 10 mm/s with 16 passes; the second group: 10 mm/s with 1 pass and 20 mm/s with 16 passes) were chosen to investigate the distortion, as shown in Fig. 7. Generally, despite the parameter combinations, laser treated surface results in distortion of the specimen, where the end of the specimen bends upwards (cf. Fig. 2). The distortion is found getting more severe as multi-pass laser hardening is conducted. By comparing the distortion with similar hardening depth, higher scanning speed with a greater number of passes experiences more distortion than the lower scanning speed and single pass.

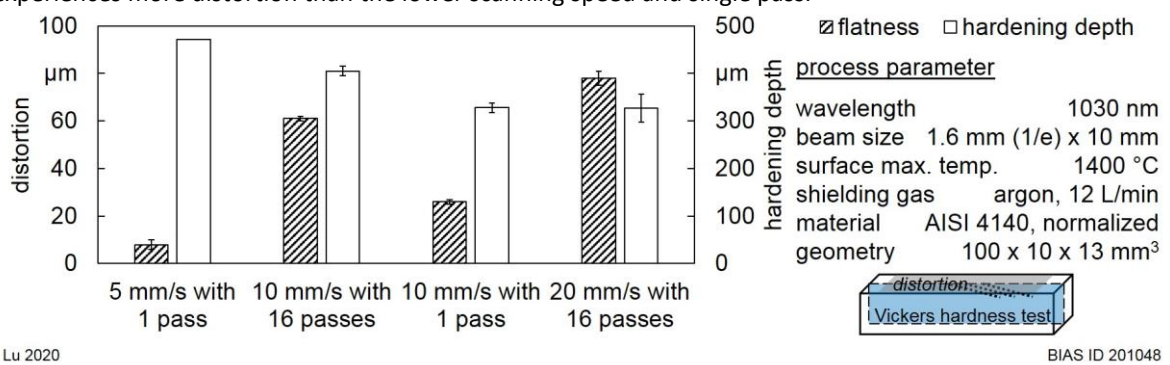

Fig. 7. Distortion after single and multi-pass laser hardening of normalized AISI 4140

4. Discussion

In this study the compressive stresses and the FWHM of diffraction peak at the surface decrease and increase in the depth of the generated martensitic zone with the number of passes. As introduced, diffraction peak broadening is particularly attributed to dislocations, microstresses, stress gradients and crystallite smallness [Ung04]. In this study, it is assumed that the peak broadening is the dominating mechanism which leads to the increase of FWHM of diffraction peak. Hence, aberrations of the peak shape and peak asymmetries, which also may influence the FWHM, are not considered. On the one hand, single pass laser hardening of steel leads to the increase of dislocation density in the hardened zone [Obe03]. On the other hand, microstresses emerge from strain incompatibilities on a microscopic scale and are usually due to the variation of yield strength, which depends on orientation of the grain and dislocation density [Pin92]. This implies the microstresses should also be induced in the laser hardening due to the variation of dislocation density in the hardened zone. In addition, in the laser hardening of AISI 4140, stress gradients are observed in the transition zone (cf. Fig. 5 and Fig. 6). This has also been observed in the transition zone with QT as initial state [Fre21].This fits to the increased FWHM of diffraction peak in the transition zone after cyclic phase transformation. Moreover, cyclic phase transformation between austenite and martensite might lead to the refinement of grain size [Nas20], and grain size in this study shows a decreasing trend as the microstructure is finer with increasing depth in the depth of the hardened zone after multi-pass laser hardening (cf. Fig. 3). However, this is not the case for grain size in the near surface. Nevertheless, the FWHM of diffraction peak seems to show the expected behavior.

The observed increased compressive residual stresses in depth with number of passes is also observed in [Kos11] and should be beneficial, as they are favorable toward higher fatigue strength and resistance to corrosion and wear [Bab19]. However, this multi-pass strategy leads to an increased distortion compared to single path with comparable hardened zone, which limit the usage of this strategy. Nevertheless, multi-pass laser hardening could be beneficial for industrial application due to a larger phase-transformed zone with higher compressive residual stresses in depth and larger hardening depth, if the increased distortion is acceptable.

5. Conclusion

Within the study on multi-pass laser hardening of AISI 4140, where there is an increase of the hardness and hardening depth, the material modifications are discussed based on the change of FWHM of diffraction peak with increasing number of paths and can be concluded as follows. The increased compressive residual stresses in the depth of the hardened zone with number of passes could be beneficial regarding the functional properties, if the increased distortion is acceptable.

Acknowledgements

The authors gratefully acknowledge the financial support for the subproject F07 and C01 funded by the Deutsche Forschungsgemeinschaft (DFG; German Research Foundation) – Projektnummer 223500200 – TRR 136.

References

[Bab19] Babu, P. D.; Marimuthu, P.: Status of laser transformation hardening of steel and its alloys: a review. Emerging Materials Research 8 (2019) 188–205

[Epp16] Epp, J.: X-ray diffraction (XRD) techniques for materials characterization. Materials Characterization Using Nondestructive Evaluation (NDE) Methods (2016) 81–124

[Fre21] Frerichs, F.; Lu, Y.; Lübben, T.; Radel, T.: Process Signature for Laser Hardening. Metals 11 (2021) 465

[Kos11] Kostov, V.; Gibmeier, J.; Wanner, A.: Local Residual Stress Distributions Induced by Repeated Austenite-Martensite Transformation via Laser Surface Hardening of Steel AISI 4140. Materials Science Forum 681 (2011) 321–326

[Kos17] Kostov, V.; Gibmeier, J.; Wanner, A.: Spatially resolved temporal stress evolution during laser surface spot hardening of steel. Journal of Materials Processing Technology 239 (2017) 326–335

[Kuh89] Kuhlmann-Wilsdorf, D.: Theory of plastic deformation: - properties of low energy dislocation structures. Materials Science and Engineering: A 113 (1989) 1–41

[Lu20] Lu, Y.; Meyer, H.; Radel, T.: Multi-cycle phase transformation during laser hardening of AISI 4140. Procedia CIRP 94 (2020) 919–923

[Mio05] Mioković, T.: Analyse des Umwandlungsverhaltens bei ein- und mehrfacher Kurzzeithärtung bzw. Laserstrahlhärtung des Stahls 42CrMo4. Schriftenreihe Werkstoffwissenschaft und Werkstofftechnik Bd. 25. Shaker Aachen (2005)

[Nas20] Nasiri, Z.; Ghaemifar, S.; Naghizadeh, M.; Mirzadeh, H.: Thermal Mechanisms of Grain Refinement in Steels: A Review. Metals and Materials International (2020)

[Nat18] Nath, A. K.; Sarkar, S.: Laser Transformation Hardening of Steel. Advances in Laser Materials Processing (2018) 257–298

[Noy87] Noyan, I. C.; Cohen, J. B.: Determination of Strain and Stress Fields by Diffraction Methods. Cohen, Jerome B. Residual stress - measurement by diffraction and interpretation (1987) 117–163

[Obe03] Obergfell, K.; Schulze, V.; Vohringer, O.: Classification of microstructural changes in laser hardened steel surfaces. Materials Science and Engineering A 355 (2003) 348–356

[Pin92] Pintschovius, L.: Macrostresses, Microstresses and Stress Tensors. Hutchings, Michael T.; Krawitz, Aaron D. Measurement of Residual and Applied Stress Using Neutron Diffraction (1992) 115–130

[Ung04] Ungár, T.: Microstructural parameters from X-ray diffraction peak broadening. Scripta Materialia 51 (2004) 777–781

[Zha03] Zhang, H.; Shi, Y.; Xu, C. Y.; Kutsuna, M.: Surface Hardening of Gears by Laser Beam Processing. Surface Engineering 19 (2003) 134–136